Computers and Concrete, *Vol. 16, No. 2 (2015) 245-260*
DOI: http://dx.doi.org/10.12989/cac.2015.16.2.245

Analysis of rectangular hybrid steel-GFRP reinforced concrete beam columns

Rafic G. El-Helou[a] and Riyad S. Aboutaha[*]

Civil and Environmental Engineering, Syracuse University, Syracuse, New York, USA

(Received August 1, 2014, Revised July 15, 2015, Accepted July 16, 2015)

Abstract. In this study, nominal moment-axial load interaction diagrams, moment-curvature relationships, and ductility of rectangular hybrid beam-column concrete sections are analyzed using the modified Hognestad concrete model. The hybrid columns are primarily reinforced with steel bars with additional Glass Fiber Reinforced Polymer (GFRP) control bars. Parameters investigated include amount, pattern, location, and material properties of concrete, steel, and GFRP. The study was implemented using a user defined comprehensive MATLAB® simulation model to find an efficient hybrid section design maximizing strength and ductility. Generating lower bond stresses than steel bars at the concrete interface, auxiliary GFRP bars minimize damage in the concrete core of beam-column sections. Their usage prevents excessive yielding of the core longitudinal bars during frequent moderate cyclic deformations, which leads to significant damage in the foundations of bridges or beam-column spliced sections where repair is difficult and expensive. Analytical results from this study shows that hybrid steel-GFRP composite concrete sections where GFRP is used as auxiliary bars show adequate ductility with a significant increase in strength. Results also compare different design parameters reaching a number of design recommendations for the proposed hybrid section.

Keywords: beam-column; GFRP; interaction diagram; ductility; moment-curvature

1. Introduction

The usage of Glass Fiber Reinforced Polymer (GFRP) reinforcing bars instead of conventional steel reinforcement has flourished during the past decade utilizing several qualities of GFRP. Corrosion resistance of GFRP makes it a suitable option in cold weather conditions where deicing chemical agents are frequently used (Toutanji and Saafi 2000). GFRP's high tensile strength, low unit weight, and equivalent thermal and stiffness characteristics provides a distinctive approach to the design and construction (Chen *et al.* 2008) of structural members. Because of its non-magnetic property, GFRP represents an alternative to steel in bridge pavements where various traffic and toll monitoring devices are used.

Adding to these distinctive properties, bond behavior of GFRP with concrete has been

[*] Corresponding author, Associate Professor, E-mail: rsabouta@syr.edu
[a] M.S., E-mail : rgelhelo@syr.edu

http://www.techno-press.org/?journal=cac&subpage=8 ISSN: 1598-8198 (Print), 1598-818X (Online)

extensively studied during the past two decades. Researchers have concluded that bond performance of GFRP to concrete depends on several factors including embedment length, concrete strength, bar diameter, bar surface properties, concrete cover, spacing between longitudinal bars, and transverse reinforcements (Baena *et al.* 2009, Ehsani *et al.* 1996, Newman *et al.* 2009, Soong *et al.* 2010). However, GFRP bond to concrete is different from that of steel bars and is related to the type of GFRP bar (Pecce 2001). The Young's modulus of the GFRP bars, namely the type of fiber, has a certain influence on the bond characteristics (Okelo *et al.* 2005). Harajli and Abouniaj (2010), Okelo *et al.* (2005), Tighiouat *et al.* (1998), and Malvar (1995) have also deduced that the bond strength between GFRP bars and concrete is significantly lower than that of steel bars. Accordingly, Eq. (1) utilizes the equilibrium principles to estimate the average bond stress (μ) at the interface between the control GFRP bars and the surrounding concrete over an embedment distance Δx, as shown in Fig. 1(a) (Aboutaha *et al.* 2012). Given their lower modulus of elasticity, under the same deformation (Fig. 1(b)), GFRP bars generate lower bond stresses at the interface with the concrete than auxiliary steel bars, thus causing significantly less damage to the column's concrete core. The bond stress at the interface between the concrete and GFRP bar is

$$\mu = \frac{D}{4\Delta x}\varepsilon_{ave}E_g \tag{1}$$

In Eq. (1), D is the diameter of GFRP bars; Δx is the embedment length of bar over which μ is being calculated; ε_{avg} is the average strain in the GFRP bar over which μ is being calculated, and E_g is the elastic modulus of GFRP bar in use.

1.1 Research significance

To prevent excessive yielding of longitudinal steel bars in reinforced concrete beam-columns, current practice provides an inner concentric steel-reinforcing cage at the end region of the beam-column as shown in Fig. 2 (Pauley and Priestley 1992, Hose *et al.* 1997). The research presented herein investigates the flexural strength and ductility of beam-column sections where GFRP bars are used as control bars instead of steel. Generating lower bond stresses at the concrete interface than steel control bars, GFRP control bars limit concrete deterioration at the core of beam-column sections and foundations of bridges where repair is not only difficult and expensive but causes bridge closure and traffic interruptions. When supported by dynamic analysis, the proposed section can be used to increase the capacity of beam-column spliced sections and column-footing interface during frequent moderate earthquakes. Adequate amount of steel transverse reinforcement is provided throughout the beam-column length to prevent shear brittle failures (Ang *et al.* 1989).

2. Research program

For the purpose of this research, a detailed analysis for a large series of rectangular column sections was conducted. These sections were reinforced with primary steel bars and GFRP control bars, as shown in Fig. 3. The investigation focused on the development of the full nominal moment-axial load (M-P) interaction diagrams, moment-curvature (M-ϕ) relationships, and curvature ductility for regular and hybrid reinforced concrete sections. The beam-columns

investigated are detailed according to current AASHTO LRFD Specifications (2012) bridge design specifications. Therefore, in the axial and bending analysis, the transverse reinforcements were assumed to be adequate to confine similar steel reinforced column section and thus, they were not investigated. Moreover, the length of the GFRP bars above the column-foundation is assumed to be at least equal to the development length (ℓ_d) of a straight GFRP bar (Fig. 2). Gradual termination of bars could also be used to minimize the physical damage in the plastic region. Aboutaha *et al.* (2011) proposed the usage of factory headed, U-shaped, or semi-circle U-shaped bars when shorter development lengths are desired. In this paper, the analysis, results, and discussions presented are for hybrid steel-GFRP rectangular column sections.

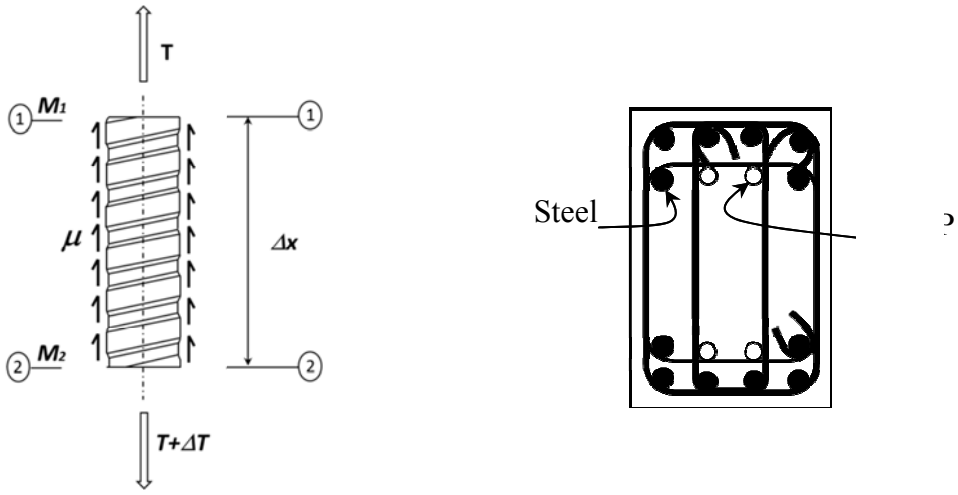

(a) Bond stress (b) Same level bars

Fig. 1 Bond stresses between a reinforcing bar and surrounding concrete

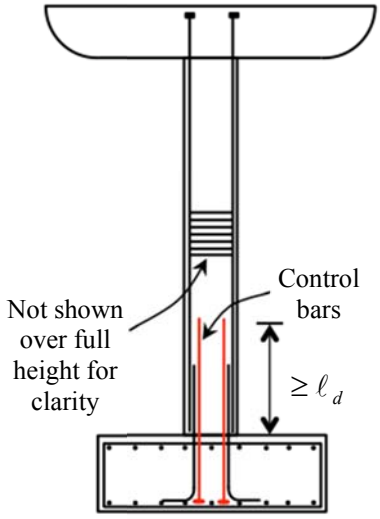

Fig. 2 Highway bridge pier with control bars

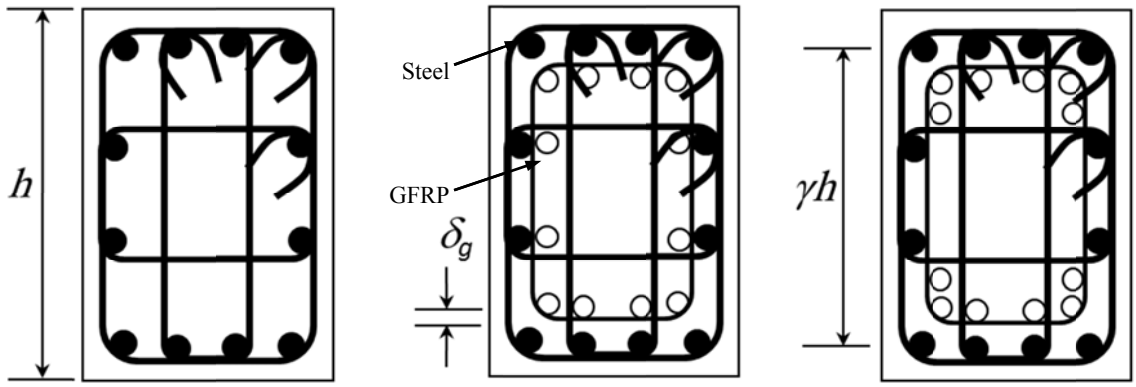

(a) Steel RC column (b) Hybrid RC column (c) Rearranged hybrid RC column

Fig. 3 Typical detailing of rectangular column sections

2.1 Geometric properties

Figs. 4 and 5 show the details of a sample of the column sections investigated in this study. While developing the M-P curves for each column section, the following variables were investigated:

(1) The amount of steel bars. Several steel reinforcement ratios were considered in the research conducted for this paper. However, for the column sections detailed in Figs. 4 and 5, a steel bar ratio (ρ_s=area of steel/gross area of concrete) of 1.33% was selected. The reference column dimensions were 2438 mm × 1219 mm, and it was reinforced with 48ϕ32 mm steel bars.

(2) The amount of the GFRP bars. Several amounts of GFRP bars were considered for each reference steel column (ρ_g=area of GFRP/gross area of concrete). The ratios of GFRP to steel bars (ρ_g/ρ_s) were set at 0.00, 0.25, 0.50, 0.75, and 1.00. The columns with GFRP control bars detailed in Fig. 4 had 12, 24, 36, or 48ϕ32 mm GFRP bars.

(3) The pattern of GFRP reinforcement. Two different patterns of reinforcement were examined in the analysis. The first pattern shown in Fig. 3(b) is the regular reinforcement pattern where the bars located at each face of the column section are equidistant. To maximize the efficiency of the GFRP bars, a non-regular pattern, termed as "rearranged", is proposed and explored. Fig. 3(c) shows the typical detailing of the rearranged pattern. The columns with GFRP control bars detailed in Fig. 5 had 12 or 36ϕ32 mm GFRP bars. For both patterns of reinforcement, the minimum bar spacing specified by AASHTO LRFD Specifications (2012) is maintained.

(4) The clear spacing between GFRP and steel bars (δ_g), measured from the main steel bars as shown in Fig. 3(b). As the GFRP bars are auxiliary bars, they were located inside the core of the column section as shown in Fig. 3. Several values for "δ_g" were considered. For the columns detailed in Figs. 4 and 5, the final adopted value was 50.8 mm, as it was the most efficient distance, and offered the largest moment arm for GFRP bars. Also, the minimum bar spacing following AASHTO Specifications (2010) was maintained.

(5) The outmost steel bar depth ratio (γ), which is the ratio of distance between centroid of outer rows of steel bars to the total depth of column section in the direction of bending, as shown in Fig. 3(c). For the sample column sections shown in Figs. 4 and 5, γ= 0.945.

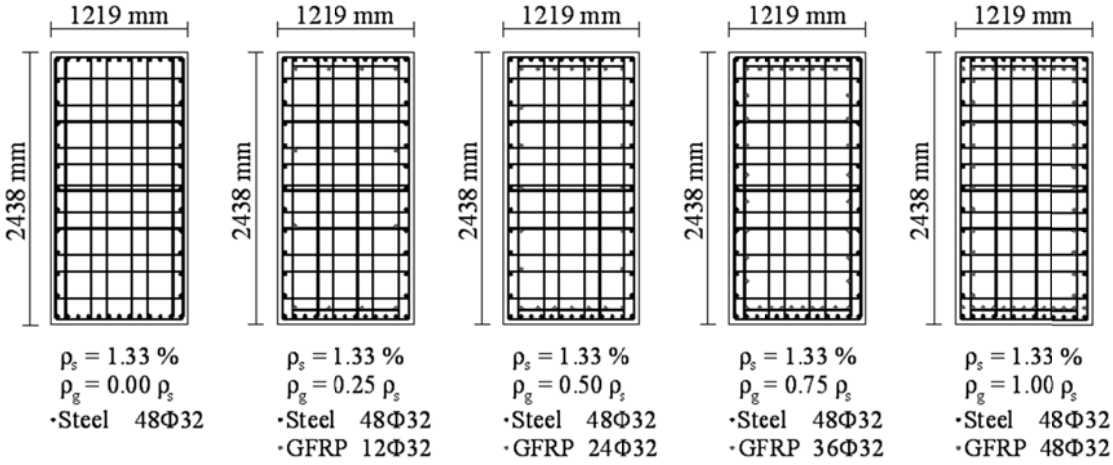

Fig. 4 Details of rectangular concrete sections with various GFRP contents using the regular reinforcement pattern (steel bars: Black; and GFRP bars: Gray)

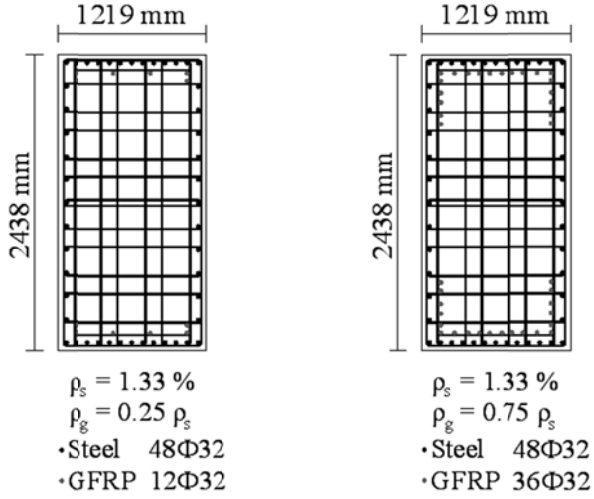

Fig. 5 Details of rectangular concrete sections with various GFRP contents using the rearranged reinforcement pattern (steel bars: Black; and GFRP bars: Gray)

2.2 Material properties

The unconfined concrete strength (f_c') chosen for this project is 41.4 MPa representing a practical strength used in bridge construction. The Modified Hognestad concrete model was used where the maximum concrete compression strain is allowed to reach ε_{cu}=0.0038. Concrete tensile strength was neglected. An idealized elasto-plastic stress-strain property was chosen for the steel bars, with yield strength (f_y) of 414 MPa and elastic modulus (E_s) of 200 GPa. The GFRP bar had an elastic response to failure, its ultimate strength (f_{gu}) was 1200 MPa, and its ultimate strain was ε_{gu}=2.0% (Aboutaha 2005). GFRP compressive strength was neglected in the analysis as its contribution at crushing of concrete is small (ACI440.1R 2006). Figs. 6(a)-6(c) shows the constitutive models for Modified Hognestad concrete, steel, and GFRP respectively. Eq. (2) was

used to model the Modified Hognestad model until the strain in the concrete reached ε_0, beyond which a linear interpolation was adopted as shown in Fig. 6(a).

$$f_c = f_c^{"}\left[\frac{2\varepsilon_c}{\varepsilon_0} - \left(\frac{\varepsilon_c}{\varepsilon_0}\right)^2\right] \tag{2}$$

In Eq. (2), ε_c is the strain in the concrete; $f_c^{"}$ and ε_0 are defined in Eqs. (3) and (4) respectively, in which E_c is the modulus of elasticity of the concrete.

$$f_c^{"} = 0.9 \times f_c \tag{3}$$

$$\varepsilon_0 = 1.8 \times \frac{f_c^{"}}{E_c} \tag{4}$$

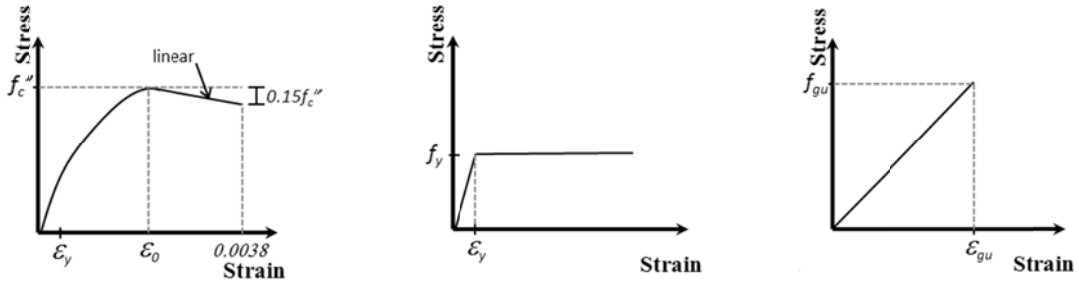

(a) Concrete (b) Steel (c) GFRP

Fig. 6 Constitutive models for concrete, steel, and GFRP (not drawn to the same scale)

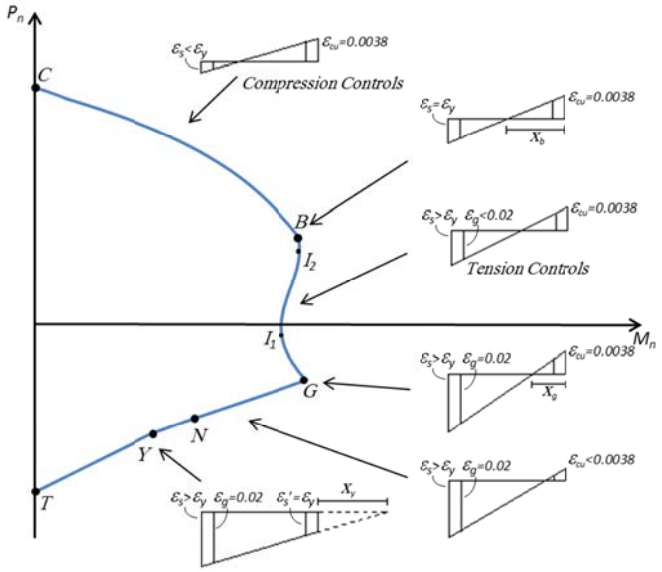

Fig. 7 Typical nominal M-P interaction diagram for a hybrid steel-GFRP section

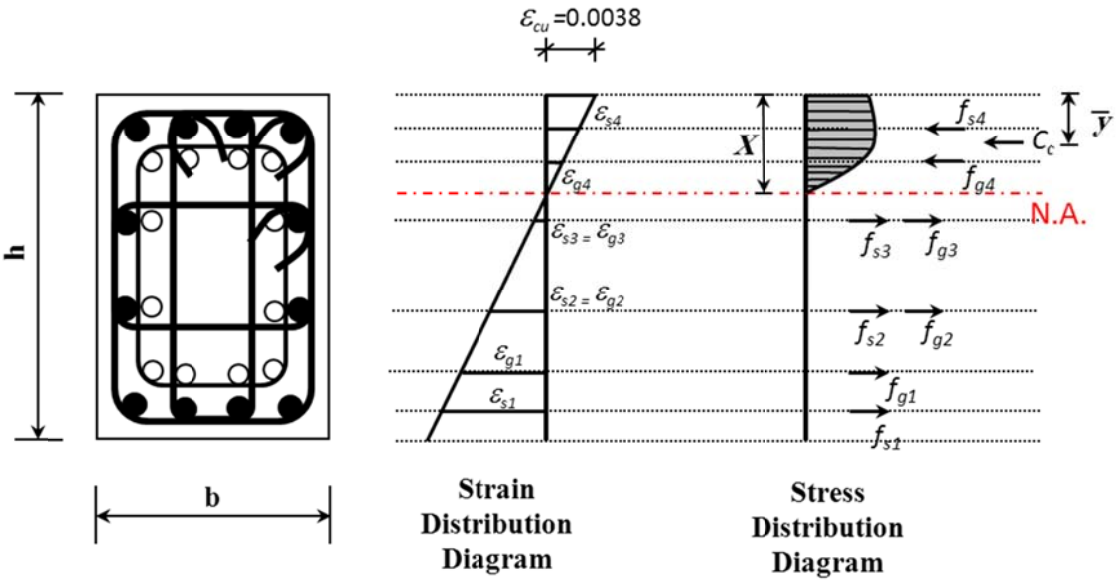

Fig. 8 Strain and stress distribution diagrams at ultimate state where maximum concrete strain is equal to 0.0038

2.3 Moment-axial load simulation model

A comprehensive MATLAB© simulation model was developed to illustrate the general solution for any rectangular section. The model is refined in such a fashion where the user would input the cross section properties and material properties of the section desired for analysis. The moment-axial load nominal strength curves (M-P interaction diagrams) were constructed for all column sections using the strain compatibility approach. In construction of the M-P diagrams, the following assumptions were adopted: (1) Plain section before bending remains plain after bending; (2) The column has adequate lateral reinforcement to provide adequate shear resistance, lateral confinement, and lateral bracing to the main longitudinal bars; and (3) Perfect bonding is maintained between steel, GFRP, and concrete.

Utilizing the strain compatibility approach and constitutive laws, the equilibrium equations were solved for every point on the M-P interaction diagram. Fig. 7 shows a typical curve of the hybrid steel-GFRP section in consideration. The leading parameter at every point was the depth of the neutral axis "*X*" ranging from negative infinity at pure axial tension, point "T", to positive infinity at pure axial compression, point "C". At point "G", the outmost tension row of the GFRP bars reached its ultimate useful strain (ε_{gu}=0.02). For the points below point "G", the compatibility equation was reconstructed by fixing the strain in the outmost tension row of the GFRP bars to its ultimate useful strain. Consequently, the strain in the top concrete fiber will be lower than its useful ultimate strain (ε_{cu}=0.0038) thereafter (El-Helou 2012).

The equilibrium equations were solved for every point of the M-P interaction diagram. The axial load (*P*) was calculated using Eq. (5), below

$$P = \sum_{i=1}^{n_s} f_{si} \times A_{si} + \sum_{i=1}^{n_g} f_{gi} \times A_{gi} + C_c \quad (5)$$

where, n_s is the total number of layers of steel reinforcement; f_{si} is the stress at each layer of steel reinforcement; A_{si} is the area of steel at each layer of reinforcement; n_g is the total number of layers of GFRP reinforcement; f_{gi} is the stress at each layer of GFRP reinforcement; and A_{gi} is the area of GFRP at each layer of reinforcement. A positive value of P indicates a compression force.

The internal moment (M) was calculated by summing the moments of all internal forces about the plastic centroid using Eq. (6), below

$$M = \sum_{i=1}^{n_s} f_{si} \times A_{si} \times (d_{pc} - d_{si}) + \sum_{i=1}^{n_g} f_{gi} \times A_{gi} \times (d_{pc} - d_{gi}) + C_c \times (d_{pc} - \bar{y}) \quad (6)$$

where, d_{si} is the depth of each layer of steel reinforcement; d_{gi} is the depth of each layer of GFRP reinforcement, $\bar{y}$ is the location of the resultant of the concrete internal compression stresses; and d_{pc} is the distance of each internal axial force measured from the plastic centroid. The plastic centroid is the location of the resultant of all internal forces, where the concrete compressive strain is uniform, and the steel strain is equal to the yield strain. For symmetrical sections, the plastic centroid is located at the center of the section. The different terms used in Eqs. (5) and (6) are illustrated in Fig. 8.

2.4 Moment-curvature simulation model

The moment-curvature (M-ϕ) relationship is obtained from curvature and the flexural moment of the beam-column section under a given load increased to failure (Olivia and Parthasarathi, 2005). For this purpose, the MATLAB® simulation codes were utilized to obtain the moment (M) and curvature (ϕ) at any specified concrete compressive strain. The purpose of this study is to plot the actual M-ϕ curve and compare it to the popular tri-linear relationship originally proposed by Park and Pauley (1975). As the GFRP reinforcements are used as auxiliary bars and located in a concentric cage at the core of the section, the yielding curvature of the hybrid section is obtained when the first tension steel yields as suggested by Park and Pauley (1975). The M-ϕ curve is linear in its initial stage; and the cracking moment is obtained using the classical elastic equation.

Flexural ductility is defined as the ability to undergo large deformations without considerable reduction in the bending moment capacity of a member (Park and Ruitong 1988). For a reinforced concrete section, ductility can be expressed in the form of curvature ductility μ_D and shown in Eq. (7).

$$\mu_D = \frac{\phi_u}{\phi_y} \quad (7)$$

In Eq. (7), ϕ_u is the curvature at ultimate state when the concrete strain reaches its limiting value (ε_{cu}), and ϕ_y is the curvature when the first layer of tension reinforcement reaches its yield capacity (f_y).

3. Discussion of the hybrid M-P curve

A detailed investigation to explain the shape of the hybrid system interaction diagram illustrated in Fig. 7 was conducted reaching the following observations

(1) At pure axial tension, point "T", the strain in the concrete section is uniform and equal to

the ultimate strain of the GFRP bars in tension (ε_{gu}=0.02).

(2) An examination has been conducted to determine the reason of the change in slope observed at point "Y". The results indicated that at this point, the top layer of steel bars has yielded, reducing the section stiffness solely to the stiffness of the GFRP bars. Consequently, when intermediate layers of steel bars yields, similar, but milder, changes in the slopes will occur as these layers have smaller amount of steel.

(3) Point "N" represents the flexural moment and axial load of the hybrid section when the depth of the neutral axis reaches zero. This point is critical in the modeling perspective of the M-P curve as it marks the start of usage of the modified Hognestad concrete model as a representation of the concrete state of stresses. For negative values of "*X*", the section would be fully under tensile strains. Yet, the tensile stresses of concrete are neglected.

(4) It can be revealed from Fig. 7 that the hybrid reinforced column section has a non-smooth continuity point "G" in the tension zone. An investigation of this point revealed that such point on the M-P curves is reached when the largest strain in the GFRP bars reaches its ultimate useful value (ε_{gu}) of 2%, as mentioned above. As this phenomenon is primarily influenced by the strain level in the GFRP bars, then the higher the amount of GFRP bars the sharper the deviation of the M-P curve, as shown in Fig. 9. Another important modeling characteristic of point "G" is that the extreme compression fiber of concrete has reached its ultimate useful strain (ε_{cu}= 0.0038). Beyond this point, the later strain is constant and the strain in the GFRP bars past this point is always less than its maximum useful value (ε_{gu}= 0.02).

(5) As shown in Fig. 8, the introduction of the GFRP bars into the section has created a "Z" shape with two inflection points "I_1" and "I_2". A detailed examination of the behavior of the M-P curve of a section reinforced with (1) a linear elastic material that can carry both tension and compression forces, (2) a linear elastic material where the compression forces are neglected, such as GFRP, and (3) a hybrid steel-GFRP section revealed that such shape is shared by all materials that have a linear elastic-to-failure mechanism. Therefore, those inflection points can be obtained by deriving the total moment "*M*" equation, shown in Eq. (6), with respect to the depth of the neutral axis "*X*" and setting it equal to zero. Using the mathematical approach of maximization and minimization, the depth of the neutral axis at those two inflection points can be obtained. However, care should be given to the values of "*X*" where the steel bars at each layer yield resulting in a change in Eq. (6) and thus changing its derivative.

(6) Point "B" of Fig. 7 shows the balanced condition where the steel bars of the bottom layer have yielded. A closer investigation on the behavior of the M-P curves near that curve revealed that the amount of the GFRP in the section influences the location the point "I_2". The lower the amount of GFRP in the section, the closer point "I_2" is to the balanced condition point "B".

(7) At pure axial compression, point "C", the section is fully under compression stresses.

4. Discussion of the M-P results

The developed M-P curves present the envelopes of the nominal capacity of the beam-column section under various axial loads and moments, as shown in Figs. 9-12. These curves could be used for any rectangular column having the same material properties, reinforcement pattern, outmost steel bar depth ratio, and ratio of steel (f_c', δ_g, f_y, γ and ρ_s), as they are non-dimensional in terms of axial stress (P/A_{gc}) and equivalent bending stress ($M/A_{gc}.h$), where "A_{gc}" and "h" are the gross cross sectional area and height of the column section, respectively.

Each M-P curve could be divided into three zones as illustrated in Fig. 9: (1) Compression control Zone "A", (2) Low axial stress ductile Zone "B", and (3) Tension control Zone "C". In the compression Zone "A", where the steel remains elastic and the GFRP bars do not carry any compressive stresses, the failure is defined by crushing of the concrete at the extreme compression fiber, at a maximum compressive strain of 0.0038. Moreover, within the zone "A", the hybrid curves coincided with the steel reinforced concrete column's curve. This was anticipated as the small compressive strength of GFRP was neglected. In the tension control Zone "C", the failure is defined by the fracture of GFRP bars and yielding of the steel reinforcement. In the low axial stress Zone "B", it is shown that for any specific axial stress (P/A_{gc}), the results suggest that an increase in the amount of the GFRP bars would lead to an increase in the bending capacity of the column section. However, the rate of increase in the bending capacity decreases as the axial stress increases, as shown in Fig. 9. The mode of failure within that region is ductile as it starts with yielding of the steel bars and then followed by crushing of the concrete. Consequently, it can be deduced that the GFRP control bars increase the bending resistance of a column section without changing its ductile mode of failure.

To maintain column ductile response during seismic events, the axial compressive stress is kept low, around or below 15% of its ultimate pure axial stress [$P \approx 0.15(A_{gc})(0.85f_c')$]. This would suggest that the GFRP bars are most effective in increasing the nominal moment capacity of a column section under compressive axial stress as it falls within Zone "B" where the GFRP is most effective. As shown in Fig. 9, for the same axial stress, an increase in the amount of GFRP control bars results in an increase in the column's bending resistance. Such increase is higher for rearranged pattern of GFRP reinforcements as shown in Fig. 10. This can be attributed to the increased moment arm and tension stress of the intermediate layers of GFRP reinforcement. However, different GFRP material properties have different impacts on the Hybrid M-P curve. Fig. 11 shows the non-dimensional nominal interaction diagrams for a subset of sections detailed Fig. 4 but with different material properties of GFRP bars. The first section is reinforced with GFRP bars having the same material properties described earlier (E_g=60 GPa, f_{gu}=1.2 GPa) and is termed as "GFRP (1)". "GFRP (2)" and "GFRP (3)" have E_g =50 GPa but different tensile strengths of f_{gu}=0.9 GPa and f_{gu} =0.4 GPa respectively. It can be inferred from Fig. 11 that as the modulus of elasticity of GFRP increases, the hybrid section flexural capacity at a specified low axial stress increases as well. That can be explained by the fact that with higher modulus of elasticity the bars can produce larger forces at a specified strain and thus higher moments are generated. However, when the ultimate tensile capacity of GFRP bar decreases at a certain modulus of elasticity, point "G", defined in Fig. 7, is shifted upward. In fact, when f_{gu} decreases, the fracture of GFRP bars occurs earlier as observed by the M-P curve of "GFRP (2)" of Fig. 11. Such situation, where point "G" is located above the moment axis, is not recommended from a design standpoint since the fracture of the column section at low axial stresses is controlled by the sudden fracture of GFRP bars. In addition to the rearranged pattern of reinforcement and type of GFRP bars, increasing the outmost depth ratio of reinforcement (γ) decreases the moment arm and stress in GFRP bars resulting in a decrease in the bending flexural capacity of the hybrid sections as shown in Fig.12.

A comparison between the interaction diagrams of a section reinforced with auxiliary GFRP bars to a section having the same amount of steel auxiliary reinforcements is illustrated in Fig. 13. The steel-steel section capacity surpasses the steel-GFRP section capacity within the compression zone, because the steel can withstand significant compression stresses while the compression strength of GFRP bars is neglected. Beyond the balanced condition, the steel-steel section capacity is also greater because of the steel's higher compression and tension capacities, and modulus of

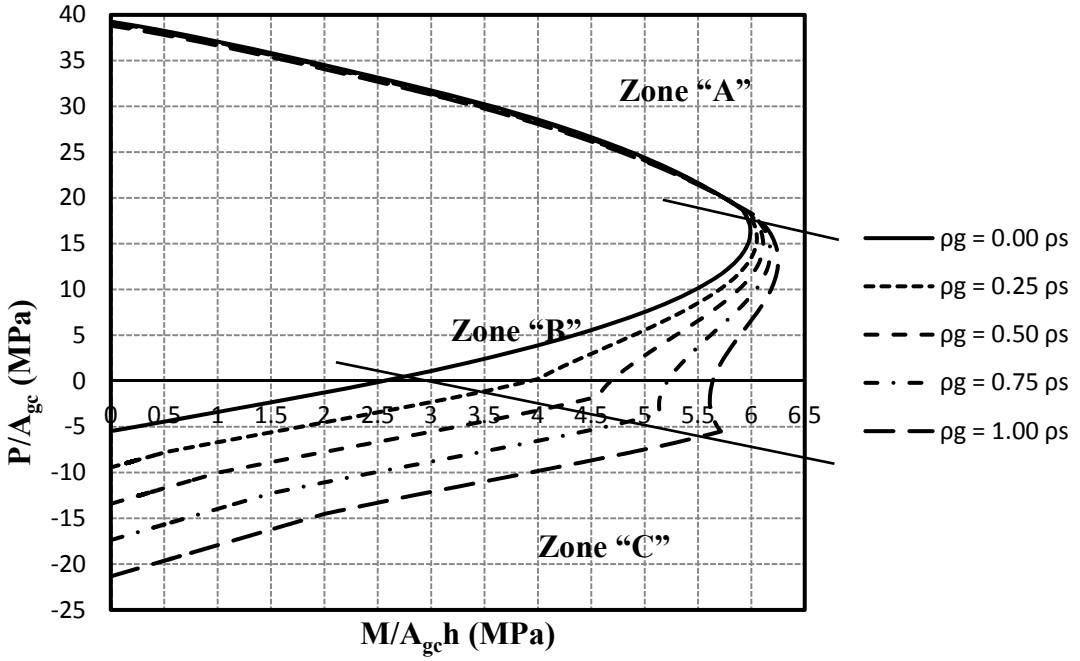

Fig. 9 Non-dimensional M-P interaction diagram for hybrid sections, f_c' = 41.4 MPa, f_y = 414 MPa, δ_g = 50.8 mm, γ = 0.945, ρ_s = 1.33%

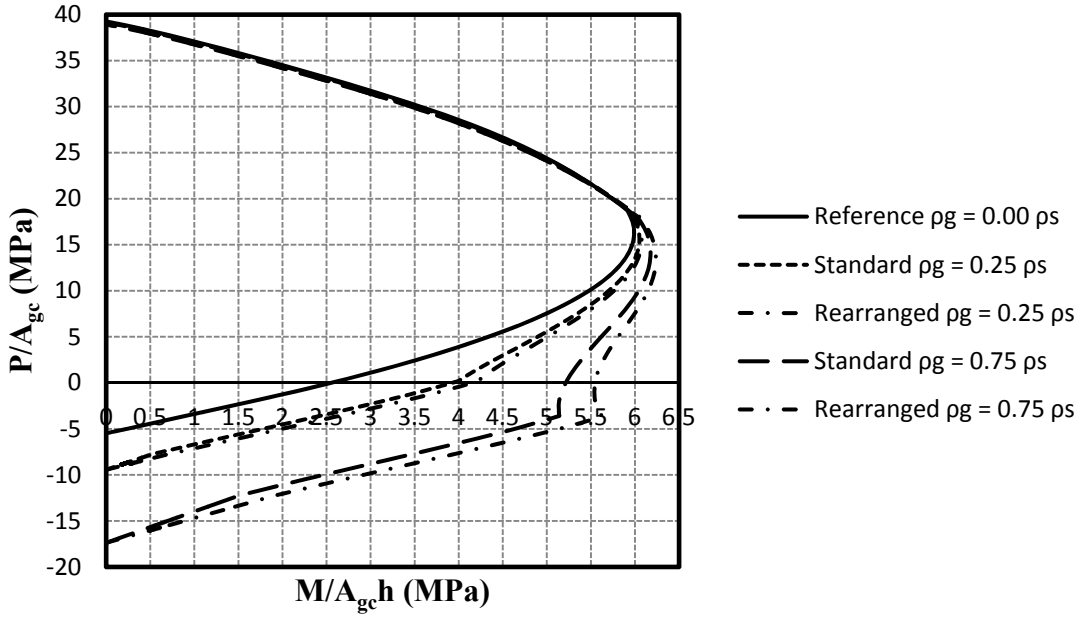

Fig. 10 Non-dimensional M-P interaction diagram for hybrid sections with standard and rearranged GFRP reinforcement pattern, f_c' = 41.4 MPa, f_y = 414 MPa, δ_g = 50.8 mm, γ = 0.945, ρ_s = 1.33%

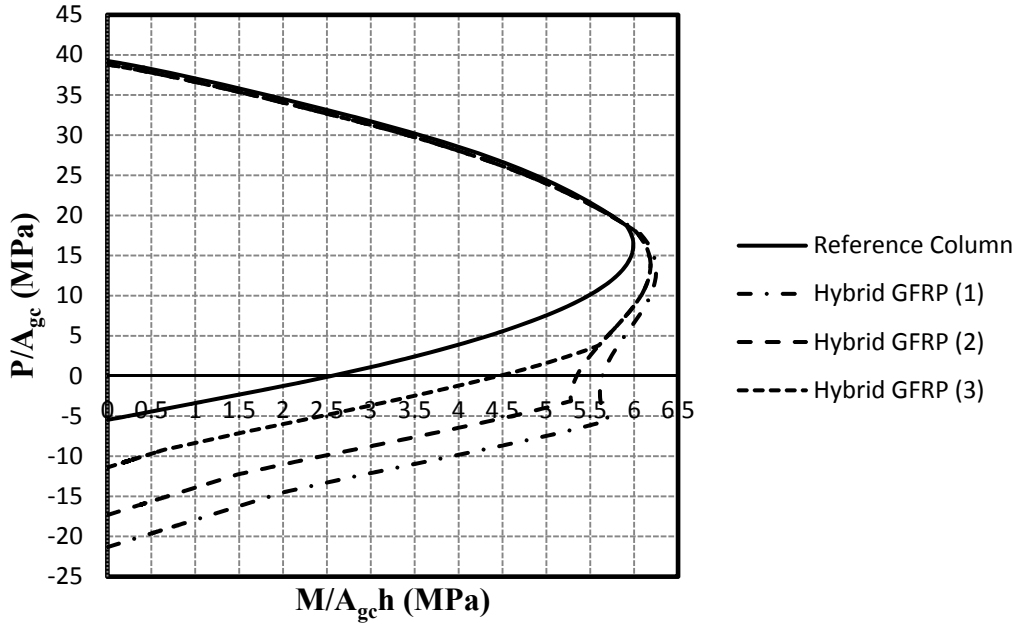

Fig. 11 Non-dimensional M-P interaction diagram for hybrid sections with different GFRP material properties, f_c' = 41.4 MPa, f_y = 414 MPa, δ_g = 50.8 mm, γ = 0.945, ρ_s = 1.33%, ρ_g = 1.00 ρ_s

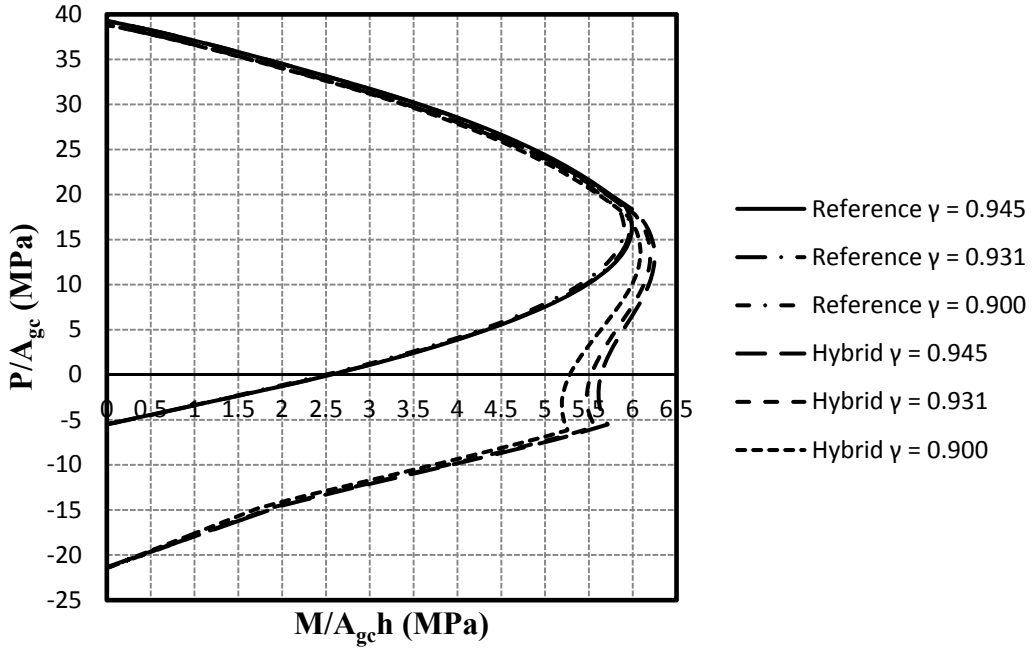

Fig. 12 Non-dimensional M-P interaction diagram for hybrid sections with different values of γ, f_c' = 41.4 MPa, f_y = 414 MPa, δ_g = 50.8 mm, γ = 0.945, ρ_s = 1.33%, ρ_g = 1.00 ρ_s

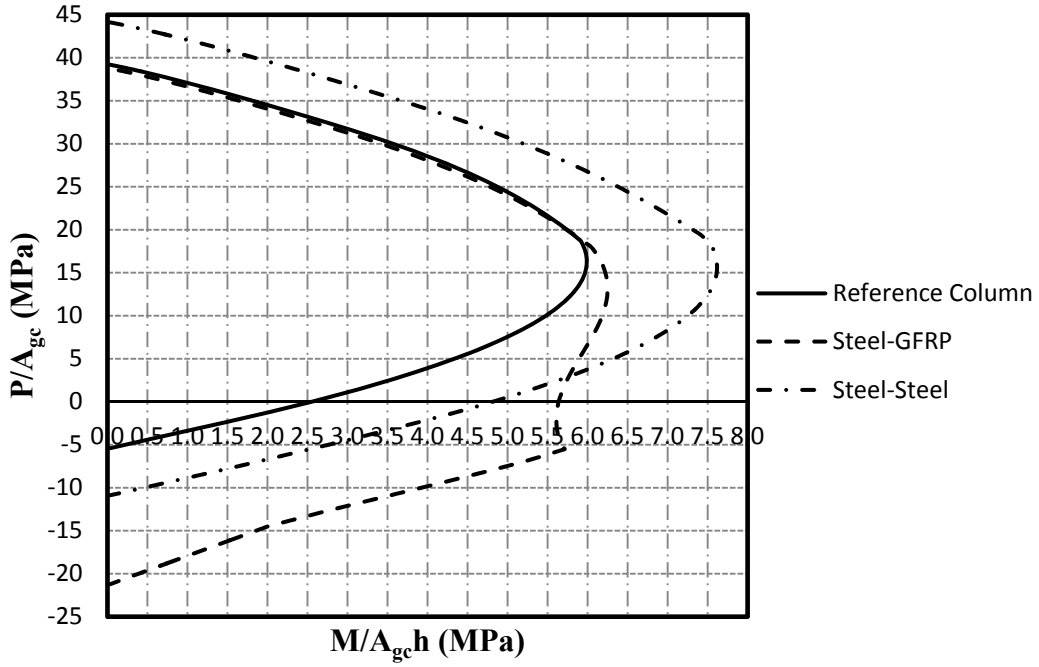

Fig. 13 Non-dimensional M-P interaction diagram for hybrid sections with the same amount of steel and GFRP auxiliary bars (f_c' = 41.4 MPa, f_y = 414 MPa, δ_g = 50.8 mm, γ = 0.945, ρ_s = 1.33%, ρ_g = 1.00 ρ_s)

elasticity compared to GFRP bars. Having a higher modulus, the steel generates higher tension stresses until reaching a strain of 0.0069 within the plastic plateau, where the stress in the GFRP becomes greater. That case occurs at low axial stresses where the steel-GFRP section capacity exceeds the steel-steel section capacity as shown in Fig. 13. Nevertheless, it should be noted that hybrid steel-GFRP sections are not studied for their ultimate capacity, but for their ability to generate lower bond stresses at the concrete interface given a certain deformation induced by moderate earthquakes. Additional parametric work on the hybrid M-P curves of the hybrid sections can be found in El-Helou (2012).

5. Discussion of ductility and M-ϕ results

The ductility results, presented in Table 1, compare the reference beam-column section ductility to the ductility of the hybrid steel-GFRP section and to another section where steel is used as auxiliary reinforcements. As shown in Table 1, the steel-GFRP sections show exceptional ductility mainly attributed to the location of the GFRP bars in the section. Positioned at the core of the beam-column section, GFRP bars allow the section to have a ductile response and to dissipate energy during cyclic deformations. As expected, ductility decreases with increasing the amount of reinforcement results (steel or GFRP) and the magnitude of the axial load. The true moment-curvature of the hybrid curve, where every point is calculated based on equilibrium

relationships, was plotted in Fig. 14 at two different axial stresses: P/A_{gc} = 0.0 MPa and P/A_{gc} = 6.9 MPa. The actual M-ϕ curves are plotted using solid lines and compared to the tri-liniar relationship, shown as dashed lines. In Fig. 14, a small break is noticed at the vicinity of the cracking moment because gradual transformation between the cracked and uncracked section was not applied.

Table 1 Ductility of the composite beam-column section using GFRP vs. steel control bars, ρ_s=1.33%, f_y=414 MPa, f_c'=41.4 MPa, δ_g = 50.8 mm, γ = 0.945

ρ_c / ρ_s ↓ \ P/A_{gc} Mpa →	0.0	1.7	3.5	5.2	6.9	Control bars
0.00	15.89	9.23	6.30	4.66	3.62	reference
0.25	9.44	6.92	5.29	4.16	3.35	GFRP
0.50	7.62	5.96	4.75	3.84	3.15	
0.75	6.65	5.35	4.36	3.59	3.00	
1.00	6.00	4.92	4.07	3.40	2.87	
0.25	12.84	8.20	5.77	4.37	3.46	Steel
0.50	10.54	7.23	5.33	4.14	3.32	
0.75	9.30	6.57	4.97	3.94	3.21	
1.00	8.22	6.05	4.69	3.77	3.10	

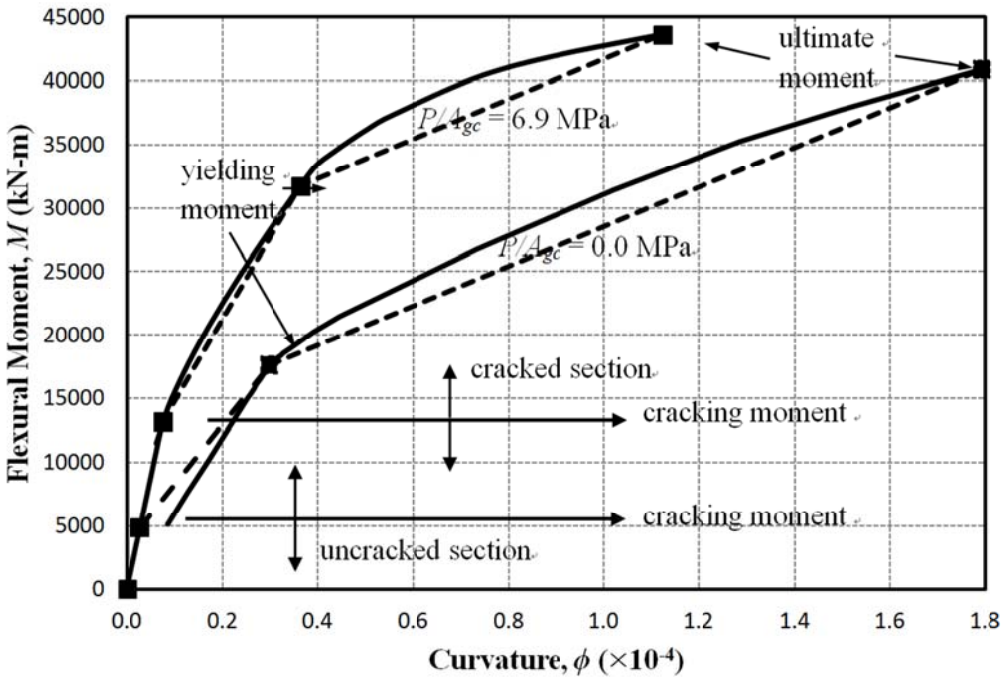

Fig. 14 True (solid lines) and tri-linear (dashed lines) M-ϕ curves at P/Agc = 0.0 MPa and P/Agc = 6.9 MPa, fc' = 41.4 MPa, fy = 414 MPa, δg = 50.8 mm, γ = 0.945, ρs = 1.33%, ρg = 1.00 ρs

6. Conclusions

The investigation presented in this paper focused on the use of GFRP as an auxiliary reinforcement to increase the capacity of beam-column sections while maintaining ductile response. For that purpose, a comprehensive analysis was performed to plot the M-P interaction diagram, the M-ϕ relationship, and ductility for the hybrid steel-GFRP section while exploring the effect of different parametric variables. Based on the results of this study, the following conclusions could be drawn

- Auxiliary GFRP bars are effective in increasing the bending capacity of rectangular steel reinforced concrete columns subjected to low axial loads (15% of ultimate pure axial stress), while maintaining ductile behavior.
- The M-ϕ curve is shown to have an exponential relationship beyond the cracking moment as opposed to the linearity suggested by Park and Pauley (1975).
- Auxiliary GFRP bars exhibit lower bond stresses at the concrete interface, as illustrated in Eq. (1) and Fig. 1, promoting further exploration in regions with moderate seismic activities for a potential to induce less damage at core of the beam-column.
- As the compressive strength of GFRP bars was neglected in the analysis, hybrid columns did not exhibit increase in the moment capacity over regular steel reinforced concrete columns subjected to high axial loads.
- Unlike steel reinforced concrete column sections, in hybrid steel-GFRP reinforced sections, a second discontinuity point in the interaction diagram is observed indicating that the ultimate strain of GFRP bars has been reached, as shown in Fig. 13.

Concrete column sections fully or partially reinforced with elastic-to-failure materials, such as GFRP, show two inflection points forming a "Z" shape in their moment-axial load interaction diagrams. A procedure to obtain the depth of the neutral axis at these inflection points was proposed.

Acknowledgements

The authors acknowledge the supports of Schöck Bauteile GmbH of Baden-Baden, Germany, Mr. Abdallah H. Yabroudi, and Mr. Abdul-Raouf Al-Bitar.

References

AASHTO (2012), "AASHTO-LRFD Bridge Design Specifications", *American Association of State Highway and Transportation Officials*, Sixth Edition, Washington DC.

Aboutaha, R.S. (2005). "Investigation of mechanical properties of ComBAR®", *Sponsored Research Report,* Syracuse University, Syracuse, NY, USA.

Aboutaha, R.S., El-Helou, R.G. and Shraideh, M.S. (2011), "Guide for the use of ComBAR® Control Rebars for Relocating Plastic Hinge Regions in Steel Reinforced Concrete Bridge Columns", *Sponsored Research Report,* Syracuse University, Syracuse, NY, USA.

Aboutaha, R.S., El-Helou, R.G. and Shraideh, M.S., (2012), "Seismic Control of Plastic Mechanism of Steel Reinforced Concrete Columns by the Use of GFRP Bars", *The Third Asia-Pacific Conference on FRP in Structures (APFIS 2012)*, The University of Hokkaido, Sapporo, Hokkaido, Japan.

American Concrete Institute (ACI) (2006), "Guide for the design and construction of structural concrete reinforced with FRP bars", *ACI 440.1R-06.*, Detroit.
Ang, B.G., Priestley, M.J.N. and Paulay, T. (1989), "Seismic shear strength of circular reinforced concrete columns", *ACI. Struct. J.*, **86**(1), 45-59.
Baena, M., Torres, L., Albert, T. and Barris, C. (2009), "Experimental study of bond behavior between concrete and FRP bars using a pull-out test", *Compo. Part. B - Eng.*, **40**(8), 784-797.
Chen, R.H.L., Choi, J.H., GangaRao, H.V. and Kopac, P.A. (2008). "Steel versus GFRP rebars?", *Federal Highway Administration*, **72**(2), FHWA-HRT-08-006.
Ehsani, M.R., Saadatmanesh, H. and Tao, S. (1996), "Design recommendations for bond of GFRP rebars to concrete", *J. Struct. Eng. - ASCE*, **122**(3), 247-254.
El-Helou, R.G. (2012), "Analysis of Rectangular Hybrid Steel-GFRP Reinforced Concrete Bridge Columns", *Master's Thesis*, Syracuse University, Syracuse, NY, USA.
Harajli, M. and Abouniaj, M. (2010), "Bond performance of GFRP bars in tension: experimental evaluation and assessment of ACI 440 guidelines", *J. Compos. Constr.*, **14**(6), 659-668.
Hose, Y., Seible, F. and Priestley, M.J. (1997), "Strategic Relocation of Plastic Hinges in Bridge Columns", *Report No. SSRP-97/05*, University of California San Diego.
Malvar, J.L. (1995), "Tensile and bond properties of GFRP Reinforcing Bars", *ACI. Struct. J.*, **92**(3), 276-285.
MATLAB© (2011) by MathWorks, http://www.mathworks.com/products/matlab/
Newman, N., Ayoub, A. and Belarbi, A. (2010), "Development length of straight FRP composite bars embedded in concrete", *J. Reinf. Plast. Comp.*, **29**, 571-589.
Okelo, R. and Yuan, R. (2005), "Bond strength of fiber reinforced polymer rebars in normal strength concrete", *J. Compos. Constr.*, **9**(3), 203-213.
Olivia, M. and Parthasarathi, M. (2005), "Curvature ductility of reinforced concrete beam", *Teknik. Sipil.*, **6**(1), 1-13.
Park, R. and Pauley, T. (1975), "*Reinforced Concrete Structures*", John Wiley & Sons., Canada
Park, R. and Ruitong, D. (1988), "Ductility of doubly reinforced concrete beam", *ACI. Struct. J.*, **85**, 217-225.
Pauley, T. and Priestley, M.J.N. (1988), "Seismic Design of Reinforced Concrete and Masonry Building", John Wiley and Sons. Inc., New York, NY, USA.
Pecce, M., Manfredi, G., Realfonzo, R. and Cosenza, E. (2001), "Experimental and analytical evaluation of bond properties of GFRP bars", *J. Mater. Civil. Eng.*, **13**(4), 282-290.
Smith, P.E. (1996), "Strategic Relocation of Plastic Hinges in Bridge Columns", *Master's Thesis*, The University of California San Diego, San Diego, CA, USA.
Soong, W.H., Raghavan, J. and Rizkalla, S.H. (2010), "Fundamental mechanisms of bonding of glass fiber reinforced polymer reinforcement to concrete", *Constr. Build. Mater.*, **25**(6), 2813-2821.
Tighiouart, B., Benmokrane, B. and Gao, D. (1998), "Investigation of bond in concrete member with fibre reinforced polymer (FRP) bars", *Constr. Build. Mater.*, **12**(8), 453-462.
Toutanji, H.A. and Saafi, M. (2000), "Flexural behavior of concrete beams reinforced with glass fiber-reinforced polymer (GFRP) bars", *ACI. Struct. J.*, **97**(72), 712-719.